Pflügers Arch - Eur J Physiol (2000) 441:398–408
DOI 10.1007/s004240000435

INSTRUMENTS AND TECHNIQUES

Ania Majewska · Glen Yiu · Rafael Yuste

A custom-made two-photon microscope and deconvolution system

Received: 26 July 2000 / Received after revision: 12 August 2000 / Accepted: 15 August 2000 / Published online: 20 October 2000

Abstract We describe in detail a custom-built two-photon microscope based on a modified confocal scanhead (Olympus Fluoview) and mode-locked Ti:sapphire laser (Coherent Mira 900). This system has internal detectors as well as external whole-field detection and an electro-optical modulator for blanking the beam on flyback and effecting fast changes in excitation intensity. This microscope can be used in deep, scattering samples for quantitative measurements with a wide range of fluorophores (GFP, fura, calcium green, calcium orange, fluo-3, DiI, DiO, fluorescein, rhodamine), for fluorescent photobleaching recovery and for uncaging. Images obtained with this system can be deconvolved with the Estimation Maximization algorithm using the program XCOSM (freeware available at: http://www.ibc.wustl.edu/bcl/xcosm/).

Keywords Fluoview · Laser · Pockels · Scanning · Spines · XCOSM

Introduction

Two-photon microscopy is a powerful tool for high-resolution imaging and photochemistry of deep scattering samples [6], and it has been recently applied to the study of dendritic spines in brain slices. Spines are very small (<1 μm in diameter) processes located on the dendrites of many neurons [15] and are sites of synaptic input [10]. These structures act as biochemical compartments [21] and allow synapses to be regulated independently. Until recently, the small size of spines has precluded their study in live tissue. The optical sectioning ability and high signal-to-noise ratio of two-photon microscopy have allowed the study of the function of spines in brain slices [20] and time-lapse morphological studies of spines in brain slices [8] and in vivo [12]. In addition, besides its imaging capabilities, two-photon excitation can be used for spatially limited fluorescence photobleaching [6], enabling multiphoton photobleaching recovery measurements (MPFPR; [3]), as well as focal uncaging or photochemistry [1, 2, 5].

Although commercial systems for two-photon microscopy are available, there are several advantages to converting an existing confocal system into a two-photon microscope [7, 13, 14, 16, 17, 18]. An important advantage is the flexibility to choose all the components of the system including the microscope, confocal unit and laser. This allows for careful tailoring of the system to the particular requirements of each application. Another important consideration is price. Commercial systems are expensive, while a do-it-yourself system can be less costly. But the most important advantage of a custom-built system is understanding its complete workings. As of today, two-photon microscopes are not yet turnkey systems and require constant maintenance. An intimate understanding of the microscope is required to determine which component needs to be realigned or replaced when a problem arises. Of course, all these advantages have to be weighed against the disadvantages of the lack of customer support and difficulties in the building of the microscope.

Methods and results

In this manuscript we want to share our experience converting a confocal system into a two-photon microscope. Our system consists of a laser set, an optical bench and a microscope (Fig. 1).

Lasers

The most common technology used to provide femtosecond pulsed IR light for two-photon microscopy is the

A. Majewska (✉) · G. Yiu · R. Yuste
Department of Biological Sciences,
Columbia University, 1212 Amsterdam Avenue,
Box 2435, New York, NY 10027, USA
e-mail: akm21@columbia.edu
Tel.: +1-212-8545023, Fax: +1-212-8658246

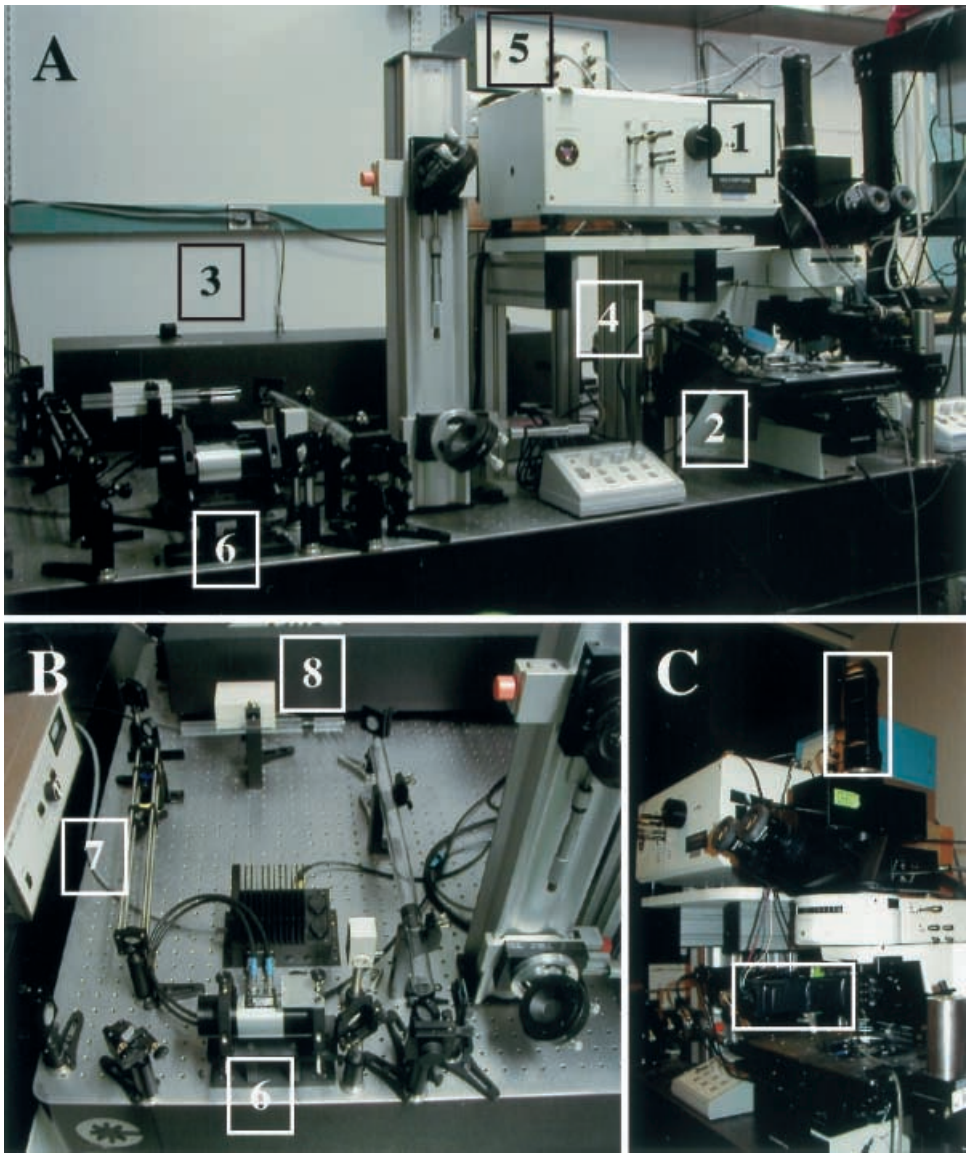

Fig. 1A–C Two-photon microscope based on a converted Fluoview scan head and the Mira Ti:Saph laser. **A** View of the two-photon set-up. (*1* Fluoview scan head, *2* Olympus upright microscope, *3* Mira Ti:sapphire laser, *4* Verdi – solid-state optical pump laser, *5* power supply and amplifier for external PMTs, *6* optical modulator.) **B** View of the beam path from the laser to the confocal scan unit. (*7* Beam shrinker, *8* Rees optical spectrum analyzer.) **C** View of the Olympus scanning unit and microscope. Notice the position of the external PMTs (*boxes*). The position on top of the microscope is used when the standard fluorescence light path needs to be used. The alternate lower position for the external PMT is least sensitive to the scattering of signal

Ti:sapphire laser, although CrLiSAF or CrLiASGAF can also be used (for a review, see [19]). In general, the most flexible (and expensive) lasers are fully tunable but difficult to operate while the least flexible but most user-friendly have a limited wavelength range. Choosing the correct laser is an important decision and the choice needs to be tailored to the application of the microscope.

We first used a CrLiASGAF laser (Flare; Clark-MXR, Mich., USA). Similar lasers are available from Time Bandwidth Products (http://iqe.ethz.ch/ultrafast). This is a small (76 cm×30 cm×15 cm) laser that easily fits on a small air table, but produces little power (<50 mW). The advantages of Cr:LisGaf lasers, new diode-pumped solid-state technology, are their lower price and small sizes. These lasers do not need an elaborate cooling system, which can often be complicated to set up and might introduce vibrations or noise. Cr:LisGaf lasers tend to be very user-friendly although, due to the low power output, they need to run at their maximum efficiency and therefore require frequent optimization of mirror settings. The average power output of our laser was 36 mW. This allowed us to obtain two-photon images of thin samples, images of mitotic spindles in *Drosophila* eggs (Fig. 2C) as well as images of GFP-labeled axons from mouse olfactory glomeruli (Fig. 2E). The main limitation of this laser, therefore, is its low power output. Although the power is sufficient for imaging bright samples and would be appropriate for applications such as time-lapse imaging of GFP-transfected cells in brain slices, it is not capable of providing a good signal-to-noise ratio for imaging dimmer samples such as in calcium measurements in indicator-filled cells in slices. To partially compensate for the low power of the laser, the optical path was minimized and the back of the objective was underfilled as opposed to the usual overfilling ([1]; see below) thus sacrificing some of the instrument's resolution.

We also tested a prototype of a compact Ti:sapphire laser (Vitesse; Coherent). This is also a small laser that is

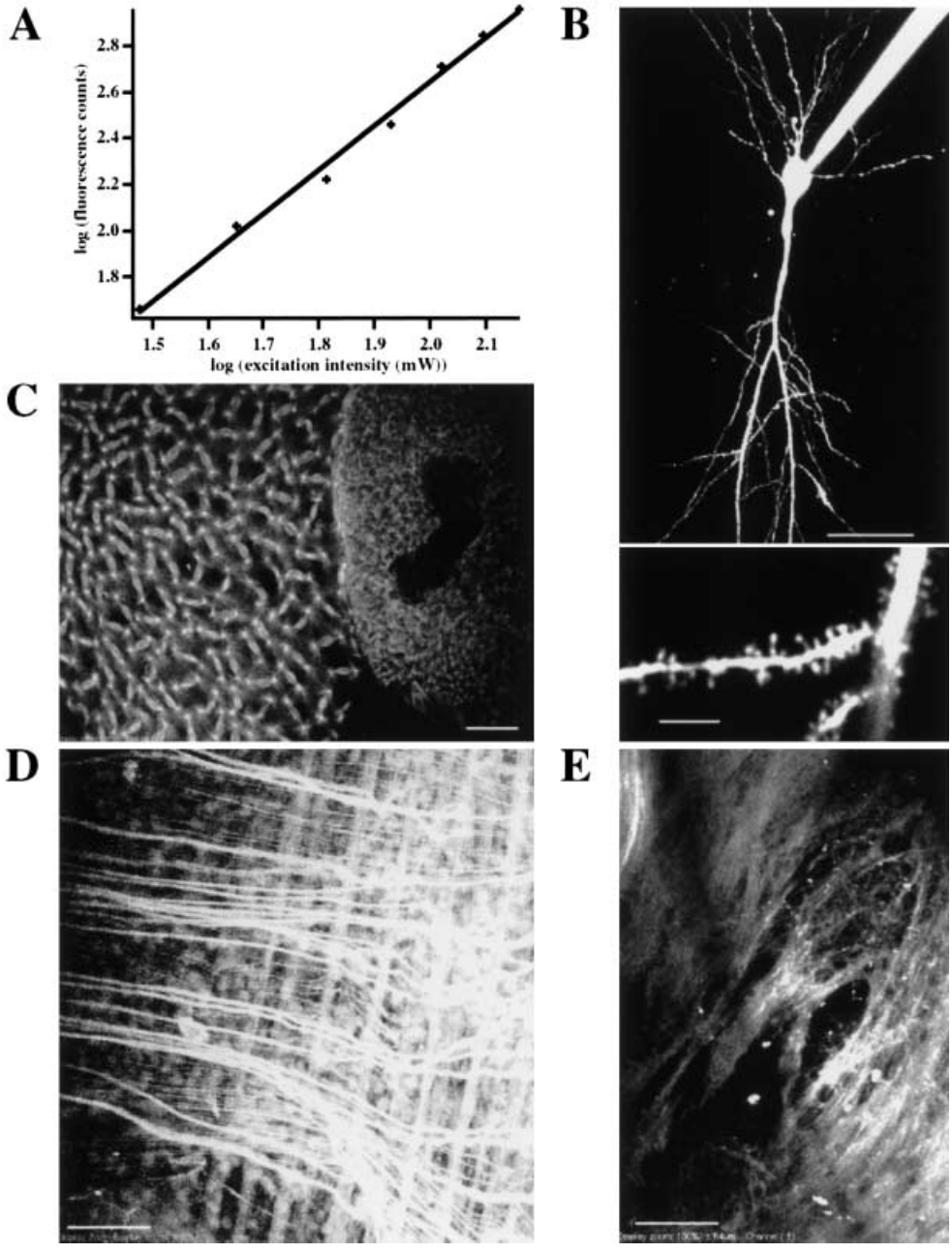

Fig. 2A–E Images acquired with the microscope. **A** Logarithmic plot of fluorescence versus excitation power. The plot has a slope of two (1.9) indicating two-photon excitation. This plot was made imaging the soma of a GFP-labeled neuron 100 µm below the surface of a cultured brain slice. A similar relationship can also be found for two-photon photobleaching. **B** A neuron filled by whole-cell perfusion with 200 µM Calcium Green–1. The neuron was located 70 µm beneath the surface of the slice. The image is a *z*-stack of individual images taken with a *z* resolution of 1 µm. *Scale bar*=50 µm. Below is an image of the boxed region of the cell taken with 10× digital zoom showing dendritic spines. This image is a *z*-stack of images taken 0.2 µm apart. *Scale bar*=5 µm. **C** *z*-stack image of rhodamine-stained mitotic spindles in a *Drosophila* egg. *Scale bar*=50 µm. **D** Images of a juvenile leech muscle stained with DiO. *Scale bar*=50 µm. **E** Image of wild-type GFP-transfected olfactory cell axons outlining a glomeruli in the olfactory bulb. *Scale bar*=100 µm

easy to use but is fixed to a single wavelength that can be determined by the user before the unit is purchased. This laser is easy to install and comes with its own diagnostics, making it easy to operate. The power output of this laser is lower than that of a regular Ti:sapphire system and limited to 200 mW. With this laser we could easily image cultured cells or cells in slices or in leech preparations up ≅100 µm deep, labeled with GFP, DiO or calcium green (Fig. 2D). Because of the small size of our room and the lack of a good ventilation system the laser did require water cooling. A disadvantage of this laser is that it is priced similarly to more powerful and flexible Ti:sapphire units.

The laser we are currently using is the Mira 900 basic – a Ti:sapphire laser from Coherent. To pump it we first used an 8-W argon laser (Innova, Coherent), which is difficult to use because of its requirement for water cooling and high voltage; we later switched to a 5-W solid-state pump laser (Verdi, Coherent). It is much smaller in size, does not require extensive cooling (a closed circuit cooler is sufficient), uses standard electrical connections and provides a high-quality beam (divergence: <0.5 mrad; power stability: ±1%, noise: <0.02% rms). According to our measurements, the 5-W Verdi produces comparable or higher powers out of the Ti:sapphire than the 8-W argon pump. This 5-W Verdi/Mira900 combination results in high powers between 700 nm and 900 nm, which are enough to both image deep samples (Fig. 2B) and do photobleaching and uncaging. We use mirror sets

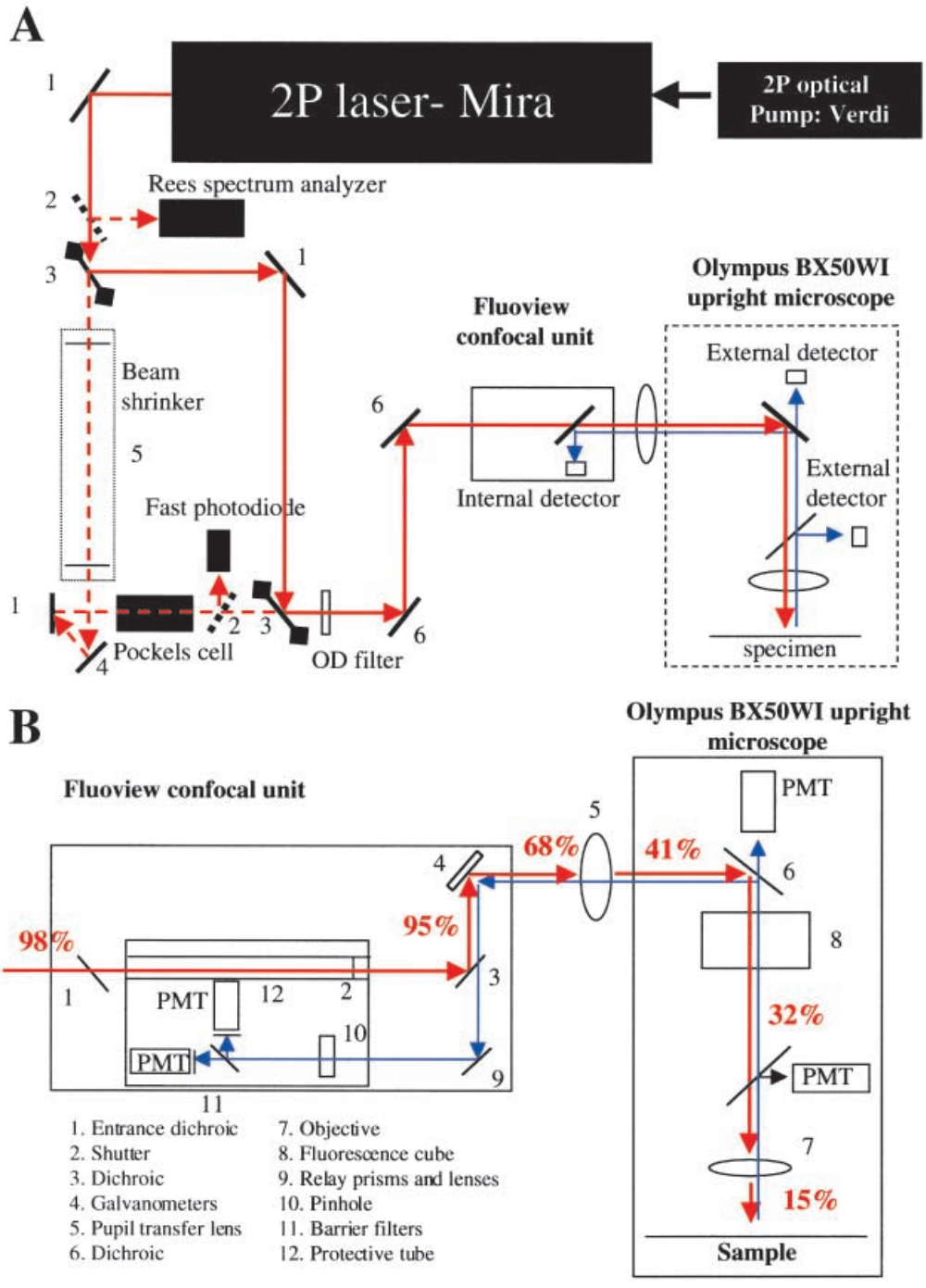

Fig. 3A, B Light path of the microscope. **A** Aerial view of the beam path. *Red arrows* indicate the path of the excitation beam while the *blue path* indicates the emission from the sample. *Solid angled lines* indicate mirrors, *broken lines* indicate coverslips that reflect a small potion of the beam and *angled lines* with *two squares* on either end indicate Flipper mirrors that can easily be taken in and out of the beam path. *Part numbers* for the numbered elements used in the beam path can be found in Table 1. The excitation beam can travel along two separate paths as shown by the *red solid* and *broken arrows*. The first path goes straight from the laser to the back of the confocal unit. The second path allows the beam to be modulated using a Pockels cell. In this case the beam must be shrunk using a lens-based beam shrinker. The ringing of the modulator can be monitored using a fast photodiode. After passing through the Pockels cell the beam joins its original path towards the confocal unit. The beam is then scanned over the sample. The emission travels back the same way as the excitation. The length of the path depends on the detector being used. **B** Beam path through the scan unit and microscope. Again, *red lines* indicate the excitation while *blue lines* show the path of the light emitted from the sample. *Red numbers* indicate the losses in the transmission of laser light incurred as the beam travels through the microscope, measured at 850 nm; comparable values were obtained at an excitation wavelength of 930 nm

dedicated to certain wavelength ranges and also a novel mirror set that allows the laser to be tuned between 700 nm and 900 nm without changing mirrors (Coherent; X-wave optics).

Laser diagnostics

As beam diagnostic devices we use a spectrum analyzer (Rees; Figs. 1, 3A) and a power meter (Powermax 500A, Molectron). A coverslip picks off a small portion of the beam (<2 mW) at the exit of the beam from the cavity and sends it into the Rees for analysis. We find this to be sufficient for maintaining a high-quality laser beam, maintaining mode locking, tuning the wavelength and determining approximate pulse durations. Alternatively, we use the internal photodiode of the Mira and an analog oscilloscope to determine modelocking.

Beam path

The elements of the two-photon microscope are laid out on a 1.8 m×1.2 m×0.2 m air table from TMC. We have

Table 1 Part numbers of elements used in the beam path between laser and confocal unit. (*Neat* New England Affiliated Technologies, *NF* New Focus, *NP* Newport, *S&H* Spindler and Hoyer, *Th* Thorlabs.) *Numbers* in *parentheses* indicated number of units used – if no number is present only one unit was used

Part number	Element
1	Mirror: NF 5103; mirror mount: Th KM1; post: Th TR-2; post holder: Th PH2-ST; base: Th BA1 (more flexible bases are available but more expensive: NF 9910+NF 9909)
2	Mirror mount: Th KM1; post: Th TR-2; post holder: Th PH2-ST; base: Th BA1; coverslip or slide attached with tape
3	Mirror mount: NF 9891; post: Th TR-2; post holder: Th PH2-ST; base: Th BA1
4	Mirror mount: NP U100-A; post: Th TR-2; post holder: Th PH2-ST; base: Th BA1
5	Beam shrinker/expander. Rods: Th ER4 (2), ER6 (8); mounting plates: Th CP02 (3); retainer rings: Th SM1RR (12); lenses: Th BPX070B, BPX085B, BPX100B; lens mounting cell: Th SM1L03 (3); shutter: SM1D12 (2)
6	Periscope. Stand: S&H 02 6106; stand cover plate: S&H 02 6212; mounting plate (mounts stand to air table): S&H 02 4330; carrier (attaches to stand and linear stage): S&H 02 6421 (2); linear stage (attaches to circular plate): Neat 1122075C (2 – bottom one for horizontal movement; top one for vertical movement); circular plate (attaches to mirror mount): S&H 02 4972 (2); mirror mount: S&H 08 5811 (2); mirror: NF 5103 (2)

two alternate beam paths that deliver the laser beam from the laser to the confocal unit (see Fig. 3A and Table 1 for elements used). One is a straight path that contains only a variable OD filter (K41–960 with mount K53–272, Edmund Scientific) while the other contains the beam shrinker and the Pockels cell (see below). The two paths are easily accessed using a Flipper mirror (PN 9891; New Focus) downstream of the laser spectrum analyzer. We use a periscope to deliver the laser beam through the back of the confocal box rather than from the side as is designed for the argon beam.

Our beam path is such that the beam overfills the back aperture of the objective without the need for a lens-based beam expander (see below). The requirement for overfilling is particularly important for quantitative measurements (such as MPFPR and uncaging) and deconvolution, and must be determined by minimizing the point spread function (PSF) of the instrument or, for a quicker, rougher analysis, simply by checking the size of the laser beam at the plane of the back aperture of the objective.

The scanning head

The Fluoview confocal unit is ideal for conversion to two-photon microscopy. It has a simple beam path (Fig. 3B), is easy to align and the unit is accessible, making it easy to modify without disturbing essential components. For its conversion to two-photon microscopy, the only components which need to be changed (Fig. 3B) are the entrance dichroic (1), separation dichroic (3), the pinhole (10), and filters (11). In addition, the side panel (next to 1) was removed and a hole was drilled to accommodate the beam without clipping. Inside the confocal unit, the first dichroic (1) was removed completely to allow the beam to enter the body of the confocal box. The beam then hits a shutter, which prevents the laser from entering the microscope when the unit is not scanning. The second dichroic (3) was changed (Chroma; 650DCSP which transmits ≅95% between 425 nm and 640 nm) to allow the beam to be reflected onto the galvanometers. The galvanometers scan the beam into the upright microscope (BX50WI, Olympus) through a transfer lens. A mirror then directs the beam downward towards the sample. In order to increase the power throughput of the unit, the transfer lens (5) was changed to a lens that has high transmission in the IR (available from Olympus). This increased the power delivered to the sample and also eliminated back-reflections of the laser light into the internal detector.

Table 2 Transmission of Olympus LUMPlanFI/IR WI objectives

Objective	800 nm	850 nm	900 nm	940 nm
40× IR1	81%	68%	8%	1%
60× IR1	74%	63%	4%	0.3%
40× IR2	77%	75%	74%	70%
60× IR2	74%	73%	71%	65%

For the return path taken by fluorescent light from the sample, the pinhole (10) was physically removed from the largest pinhole setting and IR blocking filters (BG39 Chroma) were placed in front of the internal photomultiplier tubes (PMTs). Olympus also provides two generations of 40–60× water-immersion objectives that transmit in the IR (LUMPlanFI/IR1 and 2). Transmission at different wavelengths for the old IR1 and new IR2 objectives are given in Table 2. These are ideal for electrophysiological recordings on the two-photon set-up because of their high working distances. Oil objectives with higher numerical apertures (NAs) are available for inverted microscopes. Although these objectives are more efficient for two-photon microscopy, water objectives show fewer aberrations for deep tissue imaging due to the smaller index of refraction mismatch [9], and the upright microscope allows visually guided manipulation of the sample.

Light loss through the pathway

The simple beam path and alignment of the Fluoview unit allows delivery of high light power to the sample, but major losses are encountered (Fig. 3B). These are especially important with low power lasers or for techniques that require high laser power (very deep tissue imaging, MPFPR, uncaging). The points of biggest power loss in the pathway are the galvanometers, the transfer lens and the objectives. Changing the standard transfer lens to an IR-transmitting lens provided an increase of >10% in transmission. Such considerations will become increasingly important as the excitation wavelength used becomes longer. The objectives also need to be chosen carefully. It is often necessary for the user to measure the transmission of each lens at the particular wavelength of interest. To get an accurate reading the measurement should be taken on the air table rather than in the microscope before the beam has diverged to allow the whole beam diameter to fit in the back aperture of the objective. Remember that in order to ensure the best spatial resolution (see below) the beam will be expanded by the time it hits your objective so that not all of the laser light will be transmitted through the lens, introducing further light loss.

Prism compensation

After the beam has traveled through the microscope the short pulse lengthens due to group velocity dispersion. This can be remedied using prism compensation [16]. This is an arrangement of prisms that allows the blue light, which will be retarded in glass in the microscope, a head start so that at the sample the pulse length will be maintained. Pulse broadening is a non-linear phenomenon and it is possible that the effect of prism compensation may be small. We attempted to implement prism compensation in our set up. Since it is difficult to carry out auto-correlation analyses at the sample plane, we attempted to determine the pulse duration from the fluorescence of a standard sample. We found that this method was not sufficient to allow proper prism compensation and that we could not easily determine the peak fluorescence that would correspond to the optimum prism separation even if the beam path were realigned after each prism movement. We concluded that fluctuations in alignment are greater than any gains obtained from delivering shorter pulses to the sample and decided that prism compensation is too unwieldy to use with our system on a day-to-day basis.

Internal PMT detectors

The beam path of the Fluoview is exceptionally short which limits the amount of fluorescent scattering, allowing the use of internal detectors that come with the unit. In fact using internal detectors is entirely viable for imaging deep tissue samples. Figure 2B shows an image of a pyramidal neuron in a brain slice (≅70 μm depth) taken with the internal PMT of the Fluoview. The PMT used was the R1924, which is a side-on multi-alkali PMT from Hamamatsu (Japan). Since this is a red-sensitive PMT, IR blocking filters are required. We use three kinds of filters from Chroma (BG39 for green dyes with >90% transmission from 400 nm to 550 nm; E700SP for red dyes with 90% transmission between 450 nm and 680 nm; and D550/150 especially good for highly autofluorescent samples with 85% transmission between 500 nm and 600 nm). Since 25 mm diameter filters do not fit in Olympus filter holders we affixed them to the PMT housing, although Olympus filter holders accept smaller filters that can be bought directly from Olympus.

We found that the confocal box is very prone to reflections of the IR beam. If the reflections cannot be completely blocked by the filters, it is necessary to build a protective black tube (see Fig. 3B) around the beam in the cavity where the internal PMTs are contained (K. Holthoff, pers. comm.). It is also helpful to ensure that all optics in the unit are IR compatible even if power throughput is not a concern. To minimize IR effects on the image, PMTs that are not as sensitive to red light can be used (such as bialkali PMTs; also available from Hamamatsu). To determine the voltage setting to use for the PMT we make a plot of the normalized standard deviation of the dark signal. In our case the dark noise is fairly constant until about 800 mV (Fig. 4C). It is also useful to check the linearity of the PMT by measuring the fluorescence of different low concentrations of an aqueous dye or by looking at back-scatter of the laser beam at different illumination powers.

External PMT detectors

The signal can be substantially increased by using external PMTs, which we use routinely. The PMT that we use is the HC125–02 (Hamamatsu). It is a self-contained assembly with a head-on PMT (head-on PMTs can have much larger cathode areas than side-ons) and a high voltage power supply. This is very useful as it avoids the necessity for the user to deal with high voltages. Care must be taken to ensure that the external PMT is compatible with the Fluoview hardware and software. First the output of the PMT must be comparable to the input that the confocal unit expects. This is easy to check by displaying single photon pulses from the internal PMT and those from the external PMT on an oscilloscope. In our case the external PMT pulses had a similar shape to the internal PMT ones with the Olympus preamp board but the pulses needed to be amplified (≅10×) to match the internal PMT and use the full range of the look-up tables in the Fluoview software. For this purpose we built a simple circuit using high speed op-amps to amplify the pulses ten-fold. It should be noted that the Fluoview software auto-calibrates its offset signal. This can sometimes be calibrated to a negative value, which precludes

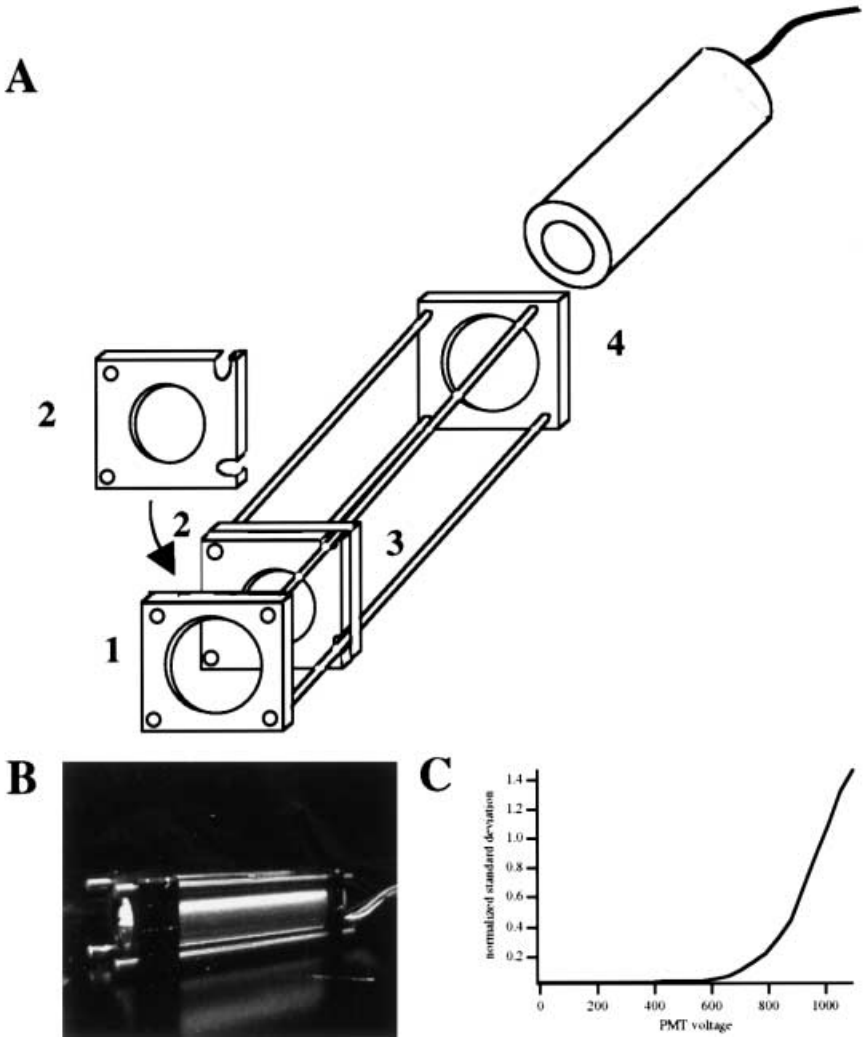

Fig. 4A–C External PMTs. **A** Schematic showing the PMT holder. This holder is easily constructed from parts available from Spindler and Hoyer. The front and back (*3*, *4*) of the PMT are held in place with set screws of two mounting plates (no. 061047). Four rods (no. 061210) connected to these plates hold the filters and the attachment to the microscope. Spindler and Hoyer provide mounting plates (*2*; no. 061024) that accommodate standard filters from Chroma (use retainer rings no. 065076 to hold the filters in place) and allow easy access to the filters by way of a swing out mechanisms. The front plate (*1*) must be modified to attach to the mount used in the microscope. **B** Photograph of the external PMT (HC125–02) in its holder. Usually this skeleton is wrapped in black electrical tape to avoid stray light hitting the photocathode. **C** Plot of the normalized dark noise of R1924 PMT (Hamamatsu) as a function of voltage

quantitative measurements and can cause loss of signal. To avoid this we disengaged the auto-calibration procedure by changing the software preferences, permanently setting the offset to a default value.

To lower the background noise we encased the HC125–02 in a protective housing, using a skeleton of Spindler and Hoyer parts covered in electrical tape and black cloth, which is both sturdy and easy to put together and manipulate (Fig. 4A, B). Spindler and Hoyer provides holders for filters that swing out and are therefore easy to change without disturbing the structure. This holder is also easy to modify to two color detection using Spindler and Hoyer parts that assemble into a cube (06 1010 –5 units; 06 1112 –8 units; 06 5058 –1 unit for rotation of dichroic during alignment; 06 5002 –1 unit which attaches to dichroic) to hold the dichroic that separates the two colors. Alternatively, the external PMT can be built using a head-on PMT with similar characteristics to the side-on internal PMT (inverted pulses, same amplitude/duration pulses). In this case the preamp boards in the Fluoview box which contain the high voltage amplifier and preamplifier can be used. This has the added advantage that voltages sent to the PMT can be adjusted directly from the software and the PMT will automatically shut off if exposed to high intensity light (this feature is built-in for the internal PMTs). This is more difficult to achieve, however, because the Olympus boards are difficult to manipulate and the user runs the risk of exposure to high voltages.

The external PMTs can be placed anywhere in the beam path of the microscope. The closer the PMT is to the sample, the less the signal is prone to scatter and the more photons will be collected. The first position that we used is on top of the upright microscope trinocular head (Fig. 1C). This required placing a dichroic (Chroma; 650DCSP which transmits ≅95% between 425 nm and 640 nm) to steer the IR laser light to the sample and the fluorescent light upwards towards the PMT. We used one of the filters from Chroma (described above) to block laser light from the PMT. In our system, the external PMT achieved a twofold increase in signal-to-noise ratio over the internal PMT. This measurement was made on thin non-scattering samples and the disparity increased with more scattering samples. We use this PMT position for samples that require fluorescence detection through the eye pieces using the standard, one-photon fluorescent

light path of the microscope. The dichroic and PMT are above the fluorescence cube and therefore do not interfere with fluorescence detection.

The second position that we use is the space right above the objective (Fig. 1C). The Olympus swinging dovetail nose piece (U-SRE) that holds the two objectives was machined and attached to a Spindler and Hoyer cube (as above, but include also 06 1621) that can hold an objective and a dichroic (Chroma; 650DCLPX which transmits ≅95% above 700 nm). The PMT housing can be easily attached to this cube. In this position the signal-to-noise ratio was 60% better then the previous external position for fluorescent signals from an indicator-loaded pipette in tissue. Again this is expected to increase for deeper tissue imaging with more light scatter. This position, however, is more prone to alignment errors and care must be taken during machining to maintain the optical axis. Also, we find that an extra IR blocking filter must be placed in front of the PMT to eliminate excitation light.

An extra improvement to increase the fluorescence signal with any PMT position is to place a mirror in the condenser beneath the sample in the rotating holder that normally holds DIC filters. This mirror (690LP Special Mirror at 0° Incidence, Chroma) reflects fluorescent light back through the sample into the PMT. For 300-µm brain slices the use of this mirror increased the signal-to-noise ratio by >15%. In thinner samples this increase might be more pronounced.

Fluoview software

The old Olympus Fluoview model that we are using implements scanning in *xy*, *xyt*, *xyz* and *xyzt* of the whole field or a region of interest. In addition it also has line scans in *xt* and *xz*, which do not allow the choice of a region of interest and are only possible in one direction. We modified the software to allow the beam to be parked in the center of the field, altering the Gbscans file by copying the code for one of the other scans and setting the xFastmultiplier, xmultiplier and ymultiplier to 0. We can then collect data from a single point in space and by doing scans collect a high number of trials (up to 8000; Fig. 5B), which can then be averaged rapidly with the Fluoview software. This is particularly useful for applications such as MPFPR and uncaging, and also if a small structure needs to be analyzed at high time resolution. Newer Fluoview models such as the FV300 or FV500 allow line scanning of angled regions of interest as well as freehand drawing of the line to be scanned in *xt* mode. The new models also have a built-in beam parking feature called point scanning and allow bidirectional scanning for better time resolution. A simple macro language is also available which should greatly increase speed and accuracy of complex procedures.

Fluoview allows data to be saved in several formats. The native format is the 12-bit Fluoview multi-TIFF, which saves all the individual scans in a stack together in one file. For image analysis we either save the images

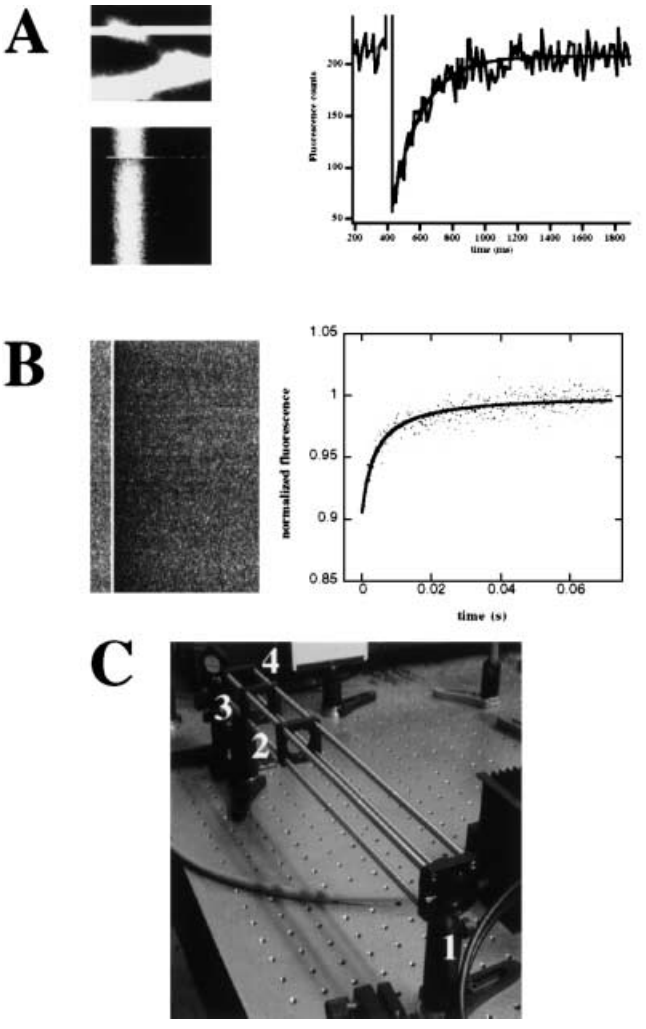

Fig. 5A–C Uses of the Pockels cell. **A** Measuring diffusional coupling between spine and dendrite using GFP-transfected neurons. The line shown in the *first panel* is scanned repeatedly to create the line scan shown in the panel below (time is on the *y*-axis). Notice that the line intersects the spine but not the dendrite. The excitation intensity is then briefly increased with the Pockels cell five- to tenfold which bleaches the molecules in the spine. Unbleached fluorophores then diffuse in from the dendrite (see *trace* on the *left*) with a characteristic time dependent on the length of the spine neck. **B** Multiphoton fluorescent photobleaching recovery in deep tissue. The beam was parked in the soma of a GFP-transfected neuron in a brain slice. Fluorescent intensities were briefly elevated (≅1 ms) to cause bleaching and the subsequent recovery was monitored. This procedure was repeated 1000 times and resulted in the image shown on the *left* where time is on the *x*-axis while trial number (1–1000) is on the *y*-axis. The plot on the *right* shows the average of all the trials with the fit of the equation from which diffusion coefficients can be obtained. **C** Schematic showing the beam shrinker/expander. Again Spindler and Hoyer parts (see Fig. 4) were used and were mounted on four rails. The first mounting plate (*1*) is attached to a lens holder and an iris used to position the beam. The second plate (*2*) holds the structure in place. The third (*3*) is attached to a lens but is not attached to the table so that it can move to allow determination of the exact distance between the lenses that maintains a parallel beam. The fourth plate (*4*) is attached to the table and holds an iris

individually in 8-bit format and do further image analysis in NIH Image (http://rsb.info.nih.gov/nih-image/) or use a newer version of NIH Image called ImageJ (http://rsb.info.nih.gov/ij/) that support Fluoview 12-bit tiffs. Fluoview also allows numerical analysis of images – such as collecting average pixel counts – and saves the data as Excel files which we later manipulate in Igor (Wavemetrics). Unfortunately the old Fluoview software does not have a macro language and the analysis can be quite time consuming. Also, Fluoview has a 3D visualization package although we have not found it particularly useful.

Fluoview does not support photon counting detection. This detection mode might be important for applications like MPFPR and uncaging where very low light levels are analyzed in order to avoid photobleaching or photodamage. In this case a separate photon counting device is required. We have used the SR430 (Stanford Research Systems) for some of our applications. The Fluoview software is still required for scanning or parking the beam but detection and analysis are done on the SR430. For photon counting where small photon fluxes are expected avalanche photodiodes may be more efficient detectors [17].

The Pockels cell

We have found the Pockels cell (Con Optics, Conn., USA) very useful both for extending specimen life and for effecting fast changes in excitation intensity. A Pockels cell is a crystal-based optical modulator, which responds to changes in voltage by instantaneously changing its transmission of light. Using voltages between 0 and 2 V we have obtained laser power ratios of 1:200 with a transmittance of 95% at the higher voltage. Two mirrors are used to direct the beam into the Pockels cell for ease of alignment. We routinely use the Pockels cell as a smart OD filter which maintains a set laser power level when data are being collected from a region of interest but blocks the laser completely when data are not being collected, such as during the time when the beam scans over structures we are not interested in or during beam flyback when the instrument does not collect data but the sample is still illuminated. We calculate that this can decrease the time of illumination of a sample between 10% and 30% depending on the scan speed used. We control the Pockels cell using a Master-8 (A.M.P.I.), a multichannel pulse generator. The Olympus confocal unit provides TTL outputs corresponding to the activation of the scan – such as scan line active and scan active – which can be used for synching external components (such as electrophysiology stimulation/acquisition and Pockels cell) with the imaging. We send the scan line active TTL to the Master-8 and in turn use the Master-8 to activate the Pockels cell to a set voltage. The duration of the Master-8 pulse can be adjusted to a duration that corresponds to the length of the line scanned or to a shorter time if the whole field is not of interest. The Master-8 can also be programmed with a delay to avoid scanning the first part of the field.

The Pockels cell can also be used to effect fast changes in laser power such as those required in photobleaching and uncaging. In this case two channels of the Master-8 are used – one to maintain monitoring power and another programmed to increase the laser power for a brief time. We use this set-up both in line scan mode where a spine is bleached to determine its coupling to the dendrite (Fig. 5A) and in parked mode where the same focal volume (usually in the soma) is monitored repeatedly for measurement of diffusion coefficients (Fig. 5B).

Because of beam divergence we find that we need to decrease the size of the laser beam before it enters the Pockels cell. For this we use a pair of lenses (10 and 20 mm focal length; BPX070B and BPX085B; Thorlabs) mounted in Spindler and Hoyer holders and rails (Fig. 5C). Using irises we guide the beam through the center of the lenses. We determine the appropriate distance between the two lenses by moving the mounts on the rails and picking the distance at which the spot on a distant wall (>3 m or 10 feet) is the smallest. Alternatively the Pockels cell can be placed closer to the laser to avoid using the beam shrinker. In some cases a beam expander after the Pockels cell might be necessary to ensure that the back aperture of the objective is overfilled. The apparatus described above can be used but the two lenses need to be switched to ensure expansion rather than reduction of beam size.

During very brief, large changes in voltage the Pockels cell can cause fluctuations of laser power (ringing). Therefore, it is important to monitor the output of the Pockels cell with a fast photodiode in quantitative applications. We use a coverslip to divert a small fraction of the beam into the photodiode and display the signal on an oscilloscope. Care must be taken to ensure that the photodiode is not saturated and background measurements (without laser) must be subtracted for an accurate reading of the magnitude of the effect. The “ringing” is minimized when the Pockels cell is well aligned and when the voltage pulses are longer in duration (>2–5 ms).

Image deconvolution

Deconvolution can be used to mathematically enhance the contrast and resolution of 3D images and allow discernment of finer structures [11]. We routinely use the program XCOSM (freeware available at: http://www.ibc.wustl.edu/bcl/xcosm/) and the Estimation Maximization algorithm [4] to deconvolve images of dendritic spines.

XCOSM software was installed in a workstation (SGI) and employed to generate an artificial widefield point spread function (WF PSF) using the optical parameters characteristic of our imaging set-up (Table 3). This was done by squaring the WF artificial PSF generated by XCOSM to create a two-photon PSF. The experimental PSFs were determined using 0.1-µm-diameter Fluores-

Table 3 Optical parameters used for deconvolution of dendritic spines and collection of experimental point spread function (*PSF*)

Parameter	Value
Distance between slices	0.1 µm
Pixel size in object space	0.033 µm
Lateral magnification	60×
Working distance	2.8 mm
Numerical aperture	0.9
Refractive index (RI) of immersion medium	1.33
Excitation wavelength	810 nm

cent Microspheres (TetraSpect; Molecular Probes) immobilized in 0.5% agarose. Images of an isolated sphere were taken at 0.1-µm intervals along the optical axis and a total of 64 slices was collected. Final PSF dimensions were $128 \times 128 \times 64$ pixels.

Images of dendritic spines were deconvolved with both the experimental PSF and the artificially generated PSF for several iterations using the XCOSM program. Results show that images deconvolved using the artificial PSF created by XCOSM preserve more structure and detail (Fig. 6B). Those deconvolved with the experimental PSF for ten iterations were in general less sharp and showed a greater loss of structures, presumably due to aberrations in the experimental PSF itself (Fig. 6C). As a control to assure that the artificial PSF is an accurate representation of the convolution of the original fluorescent sphere, the experimental PSF was deconvolved by the artificial PSF for ten iterations (Fig. 6E). The resulting image is a symmetrical sphere in all three dimensions, indicating that the artificial PSF was accurate. Images deconvolved with artificial PSFs generated with erroneous optical parameters were highly distorted (data not shown).

We found several limitations of image deconvolution of our spine data. Unfortunately, deconvolution has been shown to demonstrate bias for certain geometries. Thin structures parallel to the *X–Y* plane are more difficult to reconstruct because the spacing of planar structures may be too close to the resolution limit. In addition, the assumption of shift invariance is not a perfect depiction because points at increasing radial distances away from the central optical axis may exhibit slightly different optical parameters than points at the center of the focal plane. PSF generation is also a problem because artificial PSFs, such as one generated by XCOSM, may not account for aberrations that are intrinsic to the imaging apparatus. In the absence of aberrations, the PSF should have rotational symmetry around the optical axis and reflective symmetry about the plane of focus, as assumed by the program generating the artificial PSF. In reality, experimental PSFs are rarely symmetrical in the axial direction due to spherical aberration, which is common in imaging typical biological specimens, or incomplete alignment. Also, we found that collecting an experimental PSF is not only difficult, but can exhibit unwanted aberrations. Often, this results in the need to take many PSFs and average their pixel values. An even more important question that remains is for how many iterations can algorithms like EM be executed before parts of the original structure are lost. As shown by preliminary results (Fig. 6C), too many iterations lead to the loss of the spine neck. Future improvements should include the deconvolution of known standard structures, such as a cross or a square, to characterize how many iterations will produce the optimum result, giving the most accurate representation of the original object. Nevertheless, the prospect of using a mathematical algorithm to enhance the quality of images promises to be a useful tool. Deconvolution allows increased resolution and more accurate measurements to be taken in the small structures imaged with two-photon microscopy.

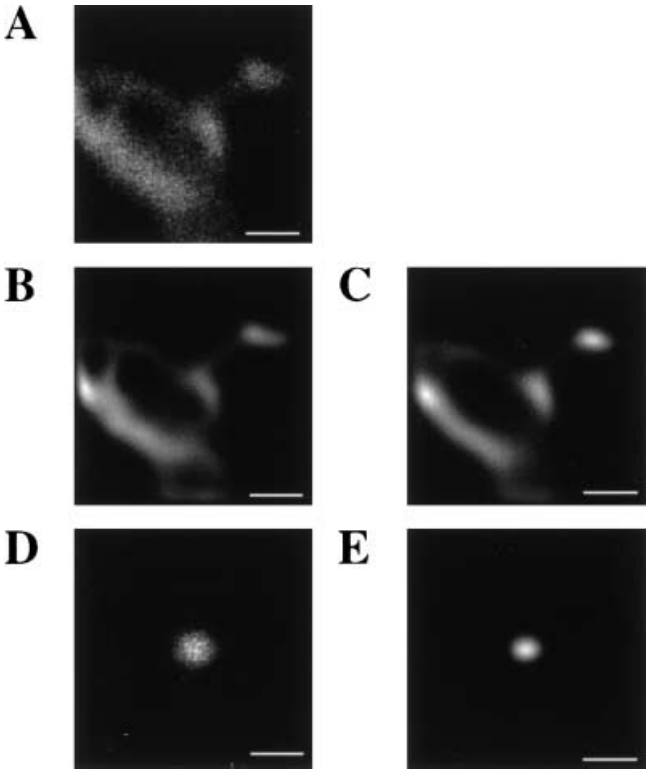

Fig. 6A–E Dendritic spine deconvolutions. **A** Original image of spine filled with 100 µM Calcium Green. **B** Image after deconvolution with an artificial point spread function (*PSF*) for ten iterations. **C** Image after deconvolution with an experimental PSF for ten iterations. **D** Experimental PSF. **E** Experimental PSF deconvolved with artificial PSF for ten iterations. *Scale bar*=1 µm

Discussion

We have described in detail a custom-built two-photon microscope based on the conversion of an Olympus Fluoview confocal unit. This conversion is relatively simple, can be accomplished in a small amount of time, and the resulting laser scanning microscope is flexible and costs less than a commercial two-photon unit. In addition, due to the simplicity of the beam path, this unit can be used for deep tissue imaging in its original conformation with descanned detection using detectors internal to the Fluo-

view scan unit. We have used three different lasers to provide excitation light and the benefits and disadvantages of each are discussed above. We describe a number of adjustments and embellishments that can make this unit more efficient and flexible. The first is the use of external, non-descanned detectors that can be placed in different positions of the beam path. These external detectors are easy to build using a Hamamatsu PMT assembly and Spindler and Hoyer elements. Care must be taken to ensure that the external PMTs are compatible with the software. Additionally, an electro-optical modulator can be used to enhance specimen survival by blanking the beam when data are not being taken and to effect fast changes in excitation intensity for applications such as MPFPR and multiphoton uncaging. This modulator can easily be synchronized with the Fluoview software. Finally, our images are deconvolved using the Estimation Maximization algorithm in XCOSM allowing improved resolution of small structures, such as dendritic spines.

We routinely use this unit for deep tissue imaging of dendritic spines in brain tissue. Additionally, we have successfully imaged different kinds of dyes with both internal and external detection. We have also been able to use the electro-optical modulator in bleaching paradigms in deep tissue that have yielded diffusion times and diffusion coefficients. Nevertheless, there are hardware and software limitations to our system that could be improved with future refinements. First, rotating line scanning or bidirectional scanning could greatly help in efficient data collection and could be implemented in the newer Fluoview systems. Also, the use of coupling lenses to the PMTs or the use of an additional PMT in the condenser position could enable even more efficient photon gathering. On that note, the use of coupling lenses to focus the light on the PMT surface could increase fluorescence detection (F. Amblard, pers. comm.). Additionally, the ability to control, via a macro language, the exact commands of the scanner could speed up the experimental protocols. Finally, the analysis should be perfected to enable the smooth importing of the 12-bit data files to programs such as ImageJ or XCOSM, to enable complete freedom to analyze and deconvolve the images, if possible in real time on the same computer.

Acknowledgements This microscope was built with the help and advice of many people in the two-photon and laser fields. In particular we would like to thank Edward Brown for help with the external detectors and many other aspects of our microscope, and Kenji Matsuba and Yoshi Kawano for invaluable help and advice. We also thank John Clark, John McKay and Gary Eisenmann for help with the lasers and David Kemp and John Lincoln for help with the Vitesse. We thank Jeff Lichtman and Fred Lanni for their advice to explore XCOSM and Jose A. Conchello and his associates for their aid in helping to resolve various problems that arose in the deconvolution process; Vijay Krishnamurthi for his advice and knowledge of the theory behind the XCOSM algorithm and Wayne Rasband for help with ImageJ. We would also like to thank Andrew Dixon, Warren Zipfel, and Knut Holthoff for discussions and Watt Webb for the loan of the SR430. We thank Tulle Hazelrigg, Peter Mombaerts and Eduardo Macagno for samples. Finally, neither ourselves nor our Department or University have any commercial interest in any of the products mentioned nor endorse their use.

References

1. Brown EB, Webb WW (1998) Two-photon activation of caged calcium with submicron, submillisecond resolution. Methods Enzymol 291:356–380
2. Brown EB, Shear JB, Adams SR, Tsien RY, Webb WW (1999) Photolysis of caged calcium in femtoliter volumes using two-photon excitation. Biophys J 76:489–499
3. Brown EB, Wu ES, Zipfel W, Webb WW (1999) Measurement of molecular diffusion in solution by multiphoton fluorescence photobleaching recovery. Biophys J 77:2837–2849
4. Conchello JA, Kim JJ, Hansen EW (1994) Enhanced three-dimensional reconstruction from confocal scanning microscope images. II. Depth discrimination versus signal-to-noise ratio in partically confocal images. Appl Opt 33:3740–3750
5. Denk W (1994) Two-photon scanning photochemical microscopy: mapping ligand-gated ion channel distributions. Proc Natl Acad Sci USA 91:6629–6633
6. Denk W, Strickler JH, Webb WW (1990) Two-photon laser scanning fluorescence microscopy. Science 248:73–76
7. Diaspro A, Corosu M, Ramoino P, Robello M (1999) Adapting a compact confocal microscope system to a two-photon excitation fluorescence imaging architecture. Microsc Res Tech 47: 196–205
8. Dunaevsky A, Tashiro A, Majewska A, Mason CA, Yuste R (1999) Developmental regulation of spine motility in mammalian CNS. Proc Natl Acad Sci USA 96:13438–13443
9. Gerritsen HC, De Grauw CJ (1999) Imaging of optically thick specimen using two-photon excitation microscopy. Microsc Res Tech 47:206–209
10. Gray EG (1959) Electron microscopy of synaptic contacts on dendritic spines of the cerebral cortex. Nature 183:1592–1594
11. Lanni F (1999) Microscopy and microscope optical systems. In: Yuste R, Lanni F, Konnerth A (eds) Imaging: a laboratory manual. Cold Spring Harbor Press, Cold Spring Harbor, pp 1.1–1.72
12. Lendvai B, Stern AE, Chen B, Svoboda K (2000) Experience-dependent plasticity of dendritic spines in the developing rat barrel cortex in vivo. Nature 404:876–881
13. Mainen ZF, Maletic-Savic M, Shi SH, Hayashi Y, Malinow R, Svoboda K (1999) Two-photon imaging in living brain slices. Methods 18:231–239
14. Potter S (1999) Two-photon microscopy for 4D in living neurons. In: Yuste R, Lanni F, Konnerth A (eds) Imaging: a laboratory manual. Cold Spring Harbor Press, Cold Spring Harbor, pp 20.1–20.16
15. Ramón y Cajal S (1891) Significación fisiológica de las expansiones protopl·smicas y nerviosas de la sustancia gris. Revista de ciencias médicas de Barcelona 22: 23
16. Soeller C, Cannell MB (1996) Construction of a two-photon microscope and optimisation of illumination pulse duration. Pflügers Arch 432:555–561
17. Tan YP, Llano I, Hopt A, Wurriehausen F, Neher E (1999) Fast scanning and efficient photodetection in a simple two-photon microscope. J Neurosci Methods 92:123–135
18. Wier WG, Balke CW, Michael JA, Mauban JR (2000) A custom confocal and two-photon digital laser scanning microscope. Am J Physiol 278:H2150–H2156
19. Wise F (1999) Lasers for two-photon microscopy. In: Yuste R, Lanni F, Konnerth A (eds) Imaging: a laboratory manual. Cold Spring Harbor Press, Cold Spring Harbor, pp 18.1–9
20. Yuste R, Denk W (1995) Dendritic spines as basic units of synaptic integration. Nature 375:682–684
21. Yuste R, Majewska A, Holthoff K (2000) From form to function: calcium compartmentalization in dendritic spines. Nature Neurosci 3:653–659